J Nanopart Res (2012) 14:1123
DOI 10.1007/s11051-012-1123-y

RESEARCH PAPER

The mechanism of cysteine detection in biological media by means of vanadium oxide nanoparticles

A. G. Bezerra Jr. · A. Barison · V. S. Oliveira · L. Foti · M. A. Krieger · R. Dhalia · I. F. T. Viana · W. H. Schreiner

Received: 10 December 2011 / Accepted: 10 August 2012

Abstract We report on the interaction of vanadate nanoparticles, produced using the laser ablation in liquids synthesis, with cysteine in biological molecules. Cysteine is a very important amino acid present in most proteins, but also because cysteine and the tripeptide glutathione are the main antioxidant molecules in our body system. Detailed UV–Vis absorption spectra and dynamic light scattering measurements were done to investigate the detection of cysteine in large biological molecules. The intervalence band of the optical absorption spectra shows capability for quantitative cysteine sensing in the μM range in biological macromolecules. Tests included cytoplasmic repetitive antigen and flagellar repetitive antigen proteins of the *Trypanosoma cruzi* protozoa, as well as the capsid p24 proteins from Human Immunodeficiency Virus type 1 and type 2. Detailed NMR measurements for hydrogen, carbon, and vanadium nuclei show that cysteine in contact with the vanadate looses hydrogen of the sulphydryl side chain, while the vanadate is reduced. The subsequent detachment of two deprotonated molecules to form cystine and the slow return to the vanadate complete the oxidation–reduction cycle. Therefore, the vanadate acts as a charge exchanging catalyst on cysteine to form cystine. The NMR results also indicate that the nanoparticles are not formed by the common orthorhombic V_2O_5 form.

Keywords Cysteine · Glutathione · Protein · Vanadate · NMR

A. G. Bezerra Jr.
Departamento Acadêmico de Física, Universidade Tecnológica Federal do Paraná, Avenida Sete de Setembro, 3165, Centro, 80230-010 Curitiba, Paraná, Brazil

A. Barison
Departamento de Química, Universidade Federal do Paraná, Centro Politécnico, Jardim das Américas, 81531-880 Curitiba, Paraná, Brazil

V. S. Oliveira · W. H. Schreiner (✉)
Departamento de Física, Universidade Federal do Paraná, Centro Politécnico, Jardim das Américas, 81531-880 Curitiba, Paraná, Brazil
e-mail: wido@fisica.ufpr.br

L. Foti · M. A. Krieger
Instituto de Biologia Molecular do Paraná, Fundação Oswaldo Cruz, Rua Professor Algacyr Munhoz Maeder, 3775, 81350-010 Curitiba, Paraná, Brazil

R. Dhalia · I. F. T. Viana
Centro de Pesquisas Aggeu Magalhães, Fundação Oswaldo Cruz, Av. Professor Moraes Rego, s/n, Campus da UFPE, Cidade Universitária, 50670-420 Recife, Pernambuco, Brazil

Introduction

Laser ablation synthesis in solution (LASiS) emerged in the last years as an alternative method to the

Published online: 23 August 2012

traditional techniques for nanoparticle accomplishment (Amendola and Meneghetti 2009). Nanoparticles are formed during the abrupt collapse of the plasma generated by the interaction of a laser pulse with a target located in a liquid. The nanoparticles can be obtained in water or solvents without stabilizing molecules. This is generally called the green synthesis, once no other byproducts are needed or formed.

Trace elements as vanadium are essential in both plants and animals. Vanadium changes its oxidation state very easily, thus leading to the wealth of oxides. The phase diagram of the vanadium–oxygen system shows some 20 oxides with many different crystal structures (Wriedt 1989). On the other hand, the interpretation of data for vanadium oxides is very difficult, especially with vanadium in biological media.

Already Macara et al. (1980) have shown that hemoglobin can reduce vanadates (Vanadium(V)) to Vanadium(IV). Their results indicated that glutathione is responsible for reducing cytoplasmic vanadate, while no enzymatic catalytic reduction mechanism is necessary.

Cysteine, Cys, is one of the 20 aminoacids found in proteins as well as in the tripeptide Glutathione (GSH). It has a thiol side-chain and is the main representative of thiols in Biology. Cys and GSH have a pivotal role in the detoxification of cells of toxic metals (see e.g., Quig 1998), as well as in the oxidation of reactive oxygen species (ROS), and oxidative stress in vivo mainly translates to GSH/Cys deficiency (see e.g., Circu and Aw 2010).

Cys has been detected in many ways, and vanadium oxides have played a role in this aspect. Teixeira et al. (2005) demonstrated the viability of the use of a carbon paste electrode, modified with an oxovanadium complex, as an amperometric sensor for Cys determination. Ji et al. (2009) used the same idea, modifying a carbon paste electrode using a molybdovanadate(V) for electrochemical Cys sensing. Thiagarajan et al. (2010) used a similar setup, using multiwalled carbon nanotubes supported on glassy carbon for amperometric Cys detection. Zhang et al. (2007) reported on a visible fluorescence method to detect cysteine/homocysteine, a technique which could be used for bioimaging, but failed to detect simple biomolecules containing Cys, such as GSH. Lim et al. (2007), as well as Lu and Zu (2007), used a different approach to detect Cys, using gold nanoparticles. It is well known that gold nanoparticles can be functionalized with this amino acid. Maduraiveeran and Ramaraj (2011) used the shift of the surface plasmon resonance of silver nanoparticles to detect Cys, adenosine and NADH.

In this way, recently we reported (Celestino-Santos et al. 2011) the possibility of detecting Cys selectively by using optical properties of a suspension of nanosized tetragonal V_2O_5 obtained by LASiS. In this work, we report on two important aspects of Cys detection with vanadium oxide nanoparticles: firstly, the possibility of detecting it quantitatively within larger biological molecules, and secondly, the experimental description of the oxi-reduction mechanism which occurs between Cys and the vanadate obtained by the LASiS process.

Experimental

A Q-switched Quantronix Model 117 Nd:YAG laser, operating at 1 kHz and delivering 200 ns pulses at 1,064 nm was used in the experiments. The laser beam was focused with a 50-mm lens on a vanadium target, Williams Advanced Materials 2N7, producing a 40-μm spot size. The laser fluence was set at 8×10^5 J/m^2. The target was placed 2 mm under bi-distilled water with a pH of 8.25, and the total water amount was maintained at 2 mL. The irradiation time was of 5 min. We measured the total amount of removed vanadium from the target by this process at 0.55 mg, which would amount to a suspension of 5.4 mM vanadium in water. The fresh nanoparticle suspension had a final pH of 4.0.

The nanoparticle size distribution was measured using a dynamic light scattering (DLS) equipment, Nanotrac NP 253 from Microtrac Inc., using 10×10 mm^2 quartz cuvettes for the suspension.

A transmission electron microscope (TEM), JEOL JEM 2010 operating at 200 kV, was employed for the micrographs. Drops of the colloidal suspension were deposited on copper grids and left to dry in air.

Atomic force microscopy (AFM) imaging was performed using a Shimadzu SPM-9500J3 microscope at room temperature. Samples were prepared depositing the suspension on atomically flat mica sheets and left to dry. Images were taken in dynamic tapping mode using NANOSENSORSTM SSS-NCHR AFM tips with a nominal spring constant of 42 N/m and a tip

radius of curvature of less than 5 nm. The scanning rate was 1 Hz and the image resolution was 256 × 256 pixels.

The UV–Vis–NIR spectra were obtained on an Ocean Optics USB 2000 spectrophotometer in the absorption mode, from 250 to 1,030 nm.

The NMR data were acquired in H_2O containing some D_2O, for lock signal, at 298 K on a Bruker AVANCE 400 NMR spectrometer operating at 9.4 Tesla, observing ^{1}H, ^{13}C, and ^{51}V nuclei at 400.13, 100.61, and 105.25 MHz, respectively, equipped with a 5-mm multinuclear direct detection probe with *z*-gradient. The ^{1}H NMR spectra were acquired with pre-saturation of the water signal during the relaxation delay. The ^{1}H, ^{13}C, and ^{51}V NMR spectra were processed by applying an exponential multiplication of the FIDs by factors of 0.3, 3.0, and 50 Hz, respectively, prior to Fourier transform, without zero-filling. The one-bond ^{1}H–^{13}C NMR correlation experiments were acquired using the gradient heteronuclear single quantum coherence (HSQC) experiment with a evolution delay of 1.1 ms for an average $^{1}J_{(H,C)}$ of 145 Hz. The $^{1}J_{(H,C)}$ experiments resulted in 2 K data points and 64 transients in t_2 for each 256 increments in t_1. The long-range ^{1}H–^{13}C correlation experiments were recorded using the gradient heteronuclear multiple bond correlation (HMBC) experiment, setting the evolution delay to 62.5 ms, optimized for $^{LR}J_{(H,C)}$ coupling constants of 8 Hz. The $^{LR}J_{(H,C)}$ experiments resulted in 2 K data points and 128 transients in t_2 for each 312 increments in t_1. All NMR chemical shifts are given in ppm (δ) related to tetramethylsilane (TMSP-d_4) signal at 0.00 ppm as internal reference for ^{1}H and ^{13}C and $VOCl_3$ signal at 0.00 ppm (neat, capillary) for ^{51}V.

The aminoacid Cys, $C_3H_7NO_2S$, Sigma-Aldrich Corporation 99 %, was first dissolved in bi-distilled water, 8.2 mM, and added to the yellowish nanoparticle suspension in 20 μL steps.

The tripeptide GSH, $C_{10}H_{17}N_3O_6S$, composed by three aminoacids Cys, glutamic acid, and glicyne (Sigma-Aldrich Corporation 99 %) was dissolved in bi-distilled water, 3.3 mM, and added to the yellowish nanoparticle suspension in 20 μL steps.

Trypanosoma cruzi genes were cloned in lambda gt11 and screened with an anti-trypomastigote antiserum. Two out of 12 clones were selected in view of their reactivity with human chagasic sera. One clone encodes a flagellar repetitive antigen (FRA) of more than 300 kDa, whereas the other corresponds to a roughly 225-kDa cytoplasmic repetitive antigen (CRA) (Table 1). The flagellar antigen is present in both epimastigotes and trypomastigotes forms, but the cytoplasmic antigen is not found in trypomastigotes. The CRA clone is entirely composed of at least 23 copies of a 42-bp repeat and the FRA gene contains at least 14 copies of a 204-bp motif. The FRA gene hybridizes to RNA of about 10 kb, while the CRA gene detects a transcript of 5.2 kb (Krieger et al. 1992).

The analyses were carried out also using the p24 capsid proteins of the Human Immunodeficiency Virus type 1 (HIV-1) and type 2 (HIV-2), whose aminoacid sequences were retrieved from the National Center for Biotechnology Information (NCBI) according to the access codes ABO61602.1 and ADI44740.1, respectively (Table 1). The p24 protein of HIV-1/2 is the most abundant viral protein, since each virus contains about 1,500–3,000 p24 molecules (Summers et al. 1992; Tang et al. 2010). During early and late stages of HIV infection, they are always present at relatively high levels in the blood, making it a potential viral marker for diagnosis, blood donor screening, monitoring disease progression, and evaluating antiretroviral therapy (Tang et al. 2010; Forsters 2003; Ly et al. 2004).

The genetic sequences encoding the HIV-1/2 p24 proteins were optimized, aiming to improve antigen expression, using the LETO 1.0 software (Entelechon®) genetic algorithm. The protein production was carried out in bacterial system, and the resultant antigens were purified through a single step of Ni-NTA affinity chromatography (QIAGEN®), followed by quantification through densitometry assays.

As can be noted, the HIV-2 p24 molecule contains twice as many Cys building blocks as HIV-1 p24, whereas Cys is absent in the CRA and FRA molecules.

Results

Nanoparticle color change

We observed the color of the freshly produced nanoparticles in water suspension at certain time intervals both visually and also acquiring the UV–Vis absorption spectra. The color of the suspension changes from dark green through blue to yellow in

Table 1 Antigen description of the proteins used in this work

Antigen	Microorganism	Aminoacid sequence	Residue number	Cys number
CRA	*T. cruzi*	QKAAEATKVAEAEK	14	0
FRA	*T. cruzi*	MEQERRQLLEKDPRRNAKEIAALEESMNARAQELAREKKLADRAFL DQKPERVPLADVPLDDDSDFVA	68	0
p24	HIV-1	MRGSHHHHHHGMASPRTLNAWVKVVEEKAFSPEVIPMFSALSEGA TPQDLNTMLNTVGGHQAAMQMLKDTINEEAAEWDRLHPVHAGPIP PGQMREPRGSDIAGTTSTLQEQIQWMTSNPPVPVGEIYKRWIILGLN KIVRMYSPVSILDIRQGPKEPFRDYVDRFFKTLRAEQATQEVKGW MTDTLLVQNANPDCKTILKALGPGATLEEMMTACQGVGGGSSCAAA	228	3
p24	HIV-2	MRGSHHHHHHGMASPRTLNAWVKLVEEKKFGAEVVPGFQALSEGCTPYDINQMLNCV GDHQAAMQIIREIINEEAAEWDVQHPIPGPLPAGQLREPRGSDIAGT TSTVEEQIQWMFRPQNPVPVGNIYRRWIQIGLQKCVRMYNPTNILDIKQGPKEPFQSYVDR FYKSLRAEQTDPAVKNWMTQTLLVQNANPDC KLVLKGLGMNPTLEEMLTACQGVGGGSSCAAA	228	6

The underline refers to cysteine units within the protein

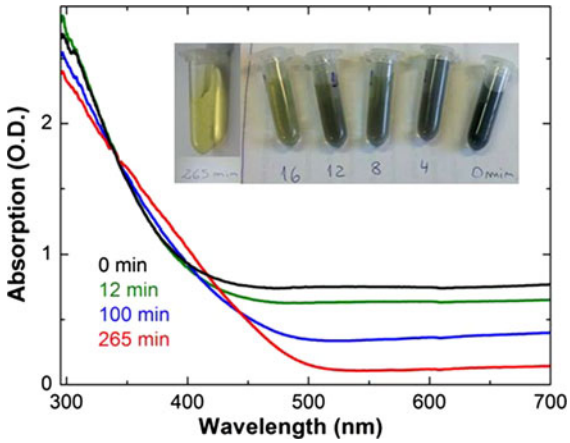

Fig. 1 UV–Vis spectra showing the oxidation of the nanoparticles at several time intervals. The *inset* shows the color of the nanoparticle suspensions

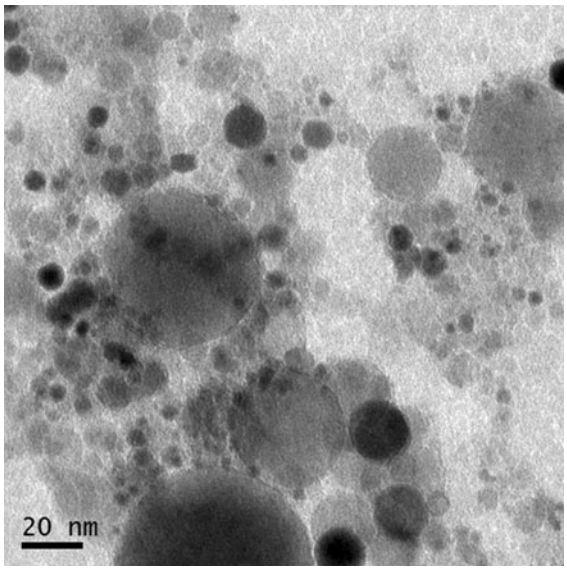

Fig. 2 TEM image of vanadate nanoparticles

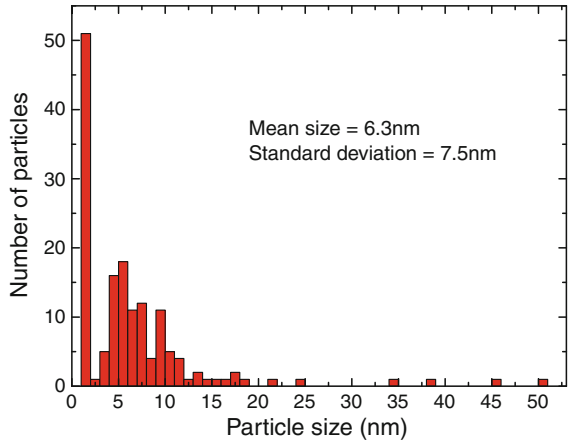

Fig. 3 Histogram corresponding to TEM image in Fig. 2

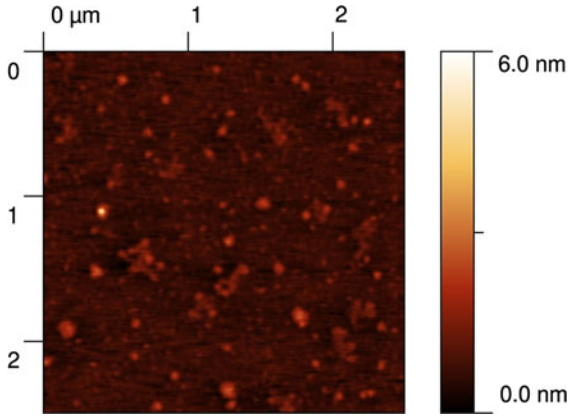

Fig. 4 AFM scan of vanadate nanoparticles on mica

several minutes, as shown in the inset of Fig. 1. The optical absorption spectra are shown in Fig. 2. Several aspects of these spectra are interesting. The absorption above 500 nm gradually diminishes with ongoing oxidation and the suspension gets more transparent. At the same time the absorption in the blue region increases, shifting the color of the suspension to yellow. Several so-called isosbestic (equal absorption at the same wavelength) points are seen in the figure. These points indicate that two different oxides with the same absorption coefficient at this wavelength are coexisting. Since the isosbestic points evolve with time, we can clearly see that the oxidation of the nanoparticles goes from lower to higher vanadium oxidation states. The necessary oxygen for this process to occur is present in the distilled water.

Nanoparticle characterization by TEM and AFM

Figure 2 shows a TEM image of the vanadate nanoparticles and Fig. 3 shows a histogram of the particle size distribution. Although there are some larger particles, the mean size is found at 6.3 nm with a rather large standard deviation of 7.5 nm. Independently of size, the nanoparticles appear mostly spherical.

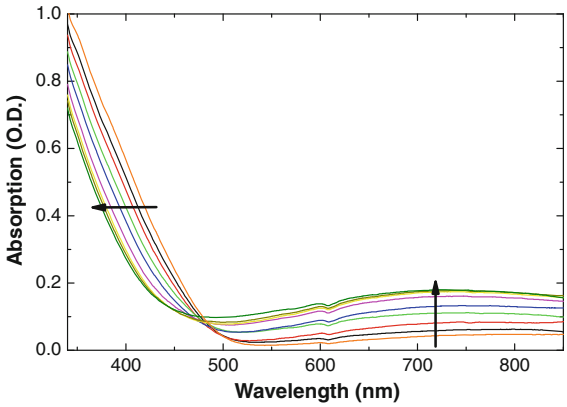

Fig. 5 Absorption spectra of the nanoparticle suspension with increasing Cys addition. The *arrows* indicate increasing Cys concentration

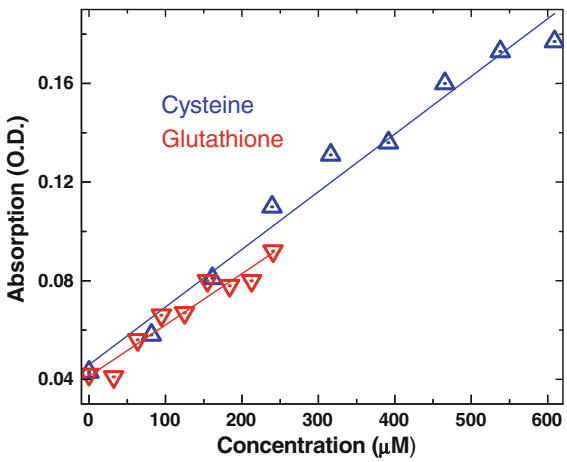

Fig. 6 Optical absorption at 720 nm versus Cys (*upright triangle*) or GSH (*inverted triangle*) concentration

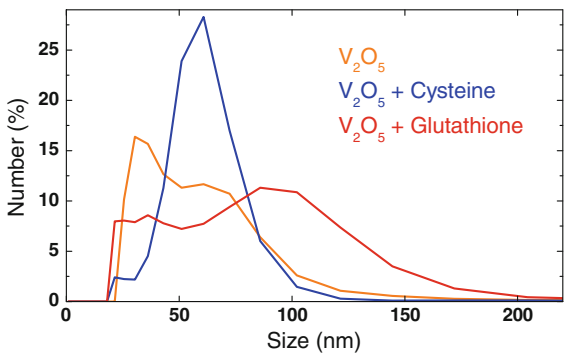

Fig. 7 Nanoparticle size distribution before and after 316 μM Cys or 240 μM GSH additions to the suspension

Figure 4 shows an AFM image of vanadate nanoparticles which after ablation were further laser milled in water suspension, where clearly a dominance of very small particles is observed.

Cysteine and glutathione

The addition of Cys to the yellowish V_2O_5 nanoparticle suspension shifts the light absorption from the blue to the UV region and the suspension gets bluish transparent with a calculated band gap of 2.87 eV (Celestino-Santos et al. 2011), while pure Cys absorbs light only in the far UV region. Figure 5 shows the typical spectra, which demonstrate a strong concentration-dependent optical absorption characteristic in the 350–480 nm region.

In addition to this color shift, a broad absorption band appears at longer wavelengths (Fig. 5). This absorption band, which is known in the literature as the intervalence band, has an intensity which also depends on the Cys concentration in the suspension. This part of the spectra was analyzed in more detail, using several Cys and GSH additions to the V_2O_5 nanoparticle suspension. The plot of the optical absorption at the 720 nm wavelength versus Cys/GSH concentration is shown in Fig. 6. A linear relationship of the optical absorption with low Cys/GSH concentrations can be observed.

Figure 7 shows the DLS nanoparticle size determinations of the raw nanoparticles and of the same added with Cys or GSH. The addition of Cys leads to a fairly large monodisperse particle distribution around 60 nm, while the addition of GSH has the effect of agglomerating some particles around 100 nm, leaving others with the original distribution around 30 nm.

Protein interaction

The CRA/FRA proteins do not contain Cys in their structure. We could detect no measurable change in the optical properties by adding both these proteins to the V_2O_5 nanoparticle suspension (data not shown).

On the other hand, when the HIV-1 and HIV-2 p24 proteins, which contain Cys in their structure, are added to the nanoparticle suspension (Fig. 8) then we find again the optical absorption of the suspension in the intervalence band region at 720 nm. A clear distinction in the absorption due to the interaction of the two proteins with the vanadium oxide

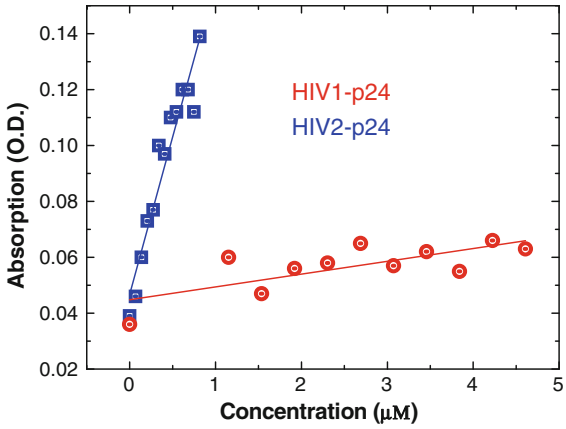

Fig. 8 Optical absorption at the 720 nm versus HIV1-p24 and HIV2-p24 concentration in the suspension

nanoparticles can be observed. The absorption at low concentrations is also linearly dependent upon concentration, but HIV-2 p24, which has twice the number of Cys molecules in its structure, shows an enhancement in the angular coefficient. Although the concentration detection is quantitative, the value of the angular coefficient could not be used to quantify Cys blocks in the protein.

Investigation of the cysteine–V_2O_5 nanoparticle interaction

The ^{51}V NMR spectra reveal that the aqueous suspension of the nanoparticles obtained by LASiS is composed mainly by a decavanadate structure $(V_{10}O_{28})^{-6}$ (V_{10}), such as that from a commercial V_2O_5 suspension (Fig. 5), although with an important additional signal at −560 ppm, which was assigned to $(V_2O_7)^{-4}$ (V_2) species (Ramasarma 2003; Crans et al. 2009) It has been known for a long time that the solvation of V_2O_5 in water leads to the decavanadate structure as well as other vanadium species depending on pH (see e.g., Ramasarma 2003). Figure 9 demonstrates clearly that the nanoparticles obtained by LASiS have a different composition from the commercial.

In relation to the addition of Cys to the aqueous nanoparticle suspension, the ^1H NMR spectra revealed that the amino acid is readily converted to another very similar compound. This fact is supported by the displacement of all NMR chemical shifts of Cys to high frequencies (Fig. 10). The signals of Cys at 3.03 (dd 14.9 and 4.1 Hz), 3.12 (dd 14.9 and 5.6 Hz) and 4.00 (dd 5.6 and 4.1 Hz) were shifted to 3.18 (dd 14.9 and 8.2 Hz), 3.39 (dd 14.9 and 3.9 Hz) and 4.13 ppm (dd 8.2 and 3.9 Hz), respectively, when added to the nanoparticle suspension obtained by LASiS. Moreover, the intensity of these new signals is gradually enhanced by increasing Cys amount in the system (Fig. 6). However, when an excess of Cys is added to the system, it seems that the new signals stop increasing and the Cys signals again emerges in the ^1H NMR spectra.

At same time the color of the solution gradually changes from a light yellow to a light transparent green-blue, showing that some alteration in the chemical structure containing vanadium is occurring during this process. The conversion of Cys into this new compound is simultaneously accomplished by the total disappearance of the three signals at −424, −505, and −525 ppm from V_{10}, as revealed in the ^{51}V NMR spectra (Fig. 11). No other signals are observed in the ^{51}V NMR spectra, indicating that the V(V) species were converted to a V(IV) species, since they are not detected by NMR.

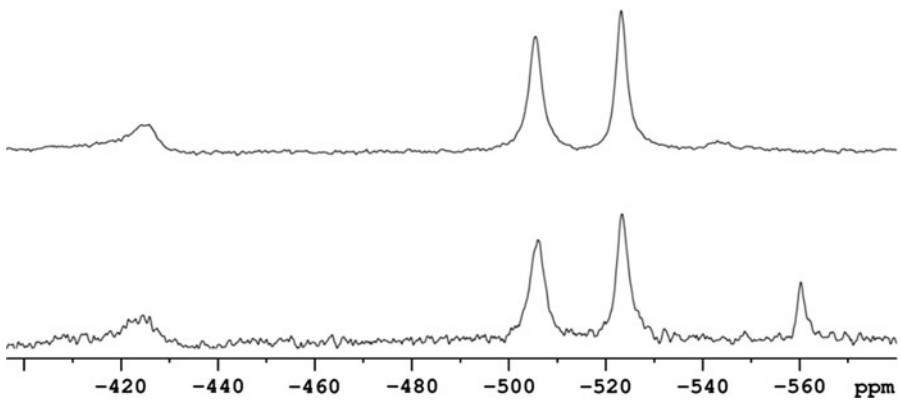

Fig. 9 ^{51}V NMR spectra from a commercial V_2O_5 suspension (*top*) and those obtained by the LASiS process (*bottom*)

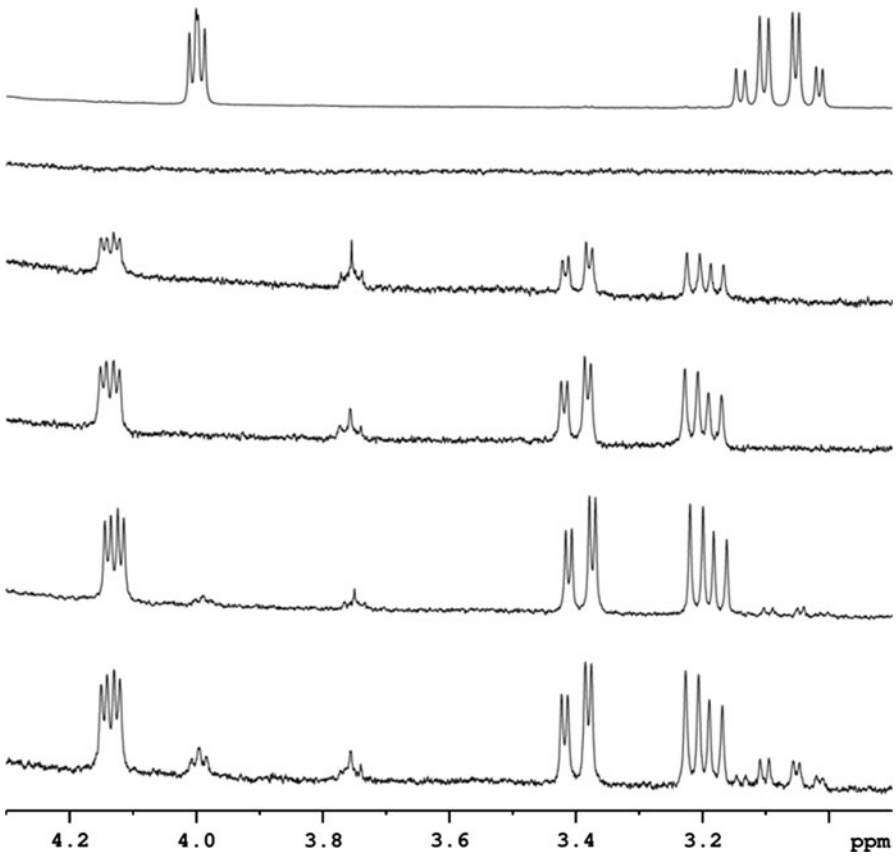

Fig. 10 ^{1}H NMR spectra from pure Cys suspension (*top*) and the gradual enhancement of a cystine signal from *top* to *bottom*

The one-bond ^{1}H–^{13}C correlation map (data not shown) from HSQC NMR experiments revealed that both hydrogen atoms of the new compound at 3.18 and 3.39 ppm are connected to the same carbon at 40.6 ppm, while the signal at 4.20 ppm is connected to carbon at 56.2 ppm. On the other hand, in the long-bond ^{1}H–^{13}C correlation map, those hydrogen atoms at 3.18 and 3.39 ppm show correlation with the carbon at 56.2 ppm, while those hydrogen atom at 4.20 ppm show correlation with the carbon at 40.6 ppm. Confronting all NMR data obtained for this new compound with those reported in the literature (Wishart et al. 1995), it was possible to confirm that the compound formed is Cystine, an oxidized form of the amino acid, which is formed by the reaction of two deprotonated Cys units (Cys–Cys).

As already noted earlier (Celestino-Santos et al. 2011) the suspension regains its yellow color after a long time. We analyzed this re-colored suspension and found a clear regeneration of the decavanadate specie, as can be observed in the ^{51}V NMR spectra (Fig. 11). The regeneration of decavanadate occurs by air oxidation, once the appearance of the yellow color starts from the top to the bottom of the solution inside the NMR tube. If the sample is kept in nitrogen atmosphere, no color change back to yellow is observed, which confirms that regeneration of the oxide occurs by air oxidation.

Discussion and conclusions

The nanoparticle formation of vanadium oxide by LASiS, starting with a vanadium target in water, is a new and easy route with a fairly high production rate with no byproducts. The nanoparticles are characterized by a tetragonal V_2O_5 structure, as shown earlier (Celestino-Santos et al. 2011), and their suspension in water leads to a quite distinct structure as compared to an orthorhombic V_2O_5 suspension, as is clearly shown in Fig. 5 of our NMR investigations. This distinction also appears in its reactivity with Cys, which is absent for a commercial V_2O_5 suspension. The ^{51}V NMR spectrum of the nanoparticle suspension indicated that

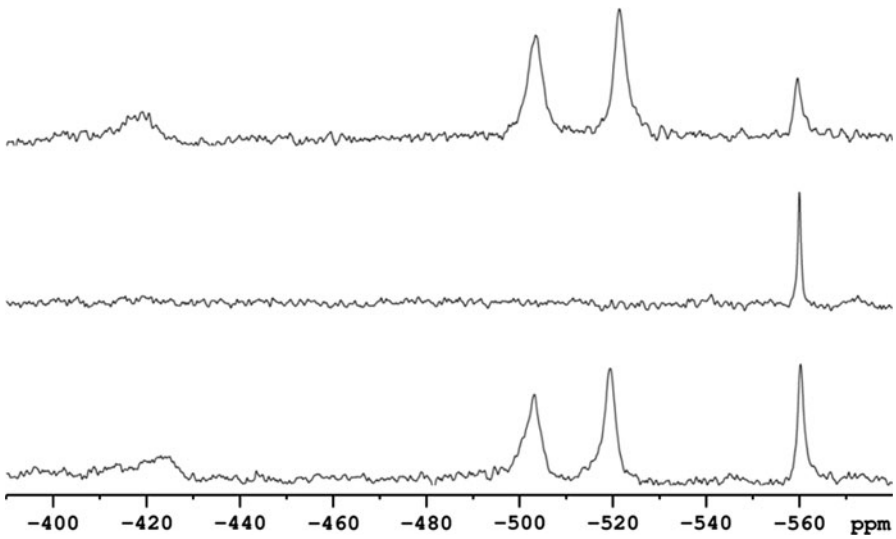

Fig. 11 ^{51}V NMR spectra before (*top*) and after (*middle*) Cys addition, and 2 weeks later (*bottom*)

there is an additional vanadium species when the nanoparticle obtained by LASiS is solvated in water, besides V_{10} species, it was also found to have V_2 species (Ramasarma 2003; Crans et al. 2009), probably due to the tetragonal V_2O_5 structure.

The interaction of the vanadium oxide nanoparticles with Cys is sensitive and completely selective, as shown here in five examples. Measuring the absorption of the intervalence band, the concentration of Cys and the tripeptide GSH can be clearly determined in the μM range. Furthermore, these small molecules seem to lead to the same relationship with Cys units in the molecules.

Bigger biological molecules, like proteins, also appear to be measurable with high sensitivity. We note that the absorption measurements are quantitative, but unfortunately the quantity of Cys blocks in the protein cannot be inferred from the data. We think that geometrical constraints hinder a complete Cys block quantification. The folding of proteins, together with the size relationship of molecules versus nanoparticles, are the probable causes of this hindrance.

The chemistry of the interaction of the V_2O_5 nanoparticles with the amino acid could be followed with NMR measurements. Our findings show that there occurs the oxidation of Cys, which looses one hydrogen atom of the sulphydril side chain, followed readily by a bonding of two deprotonated molecules in order to form cystine. The nanoparticles, on the other hand, gradually reduce their vanadium V content, depending on Cys concentration, forming vanadium IV in this reaction. Therefore, it can be concluded that the reaction to form cystine from Cys is catalyzed by the vanadium oxide nanoparticles.

The formation of cystine from Cys is a natural process that occurs reversibly in cells. The same mechanism applies to GSH (GSH–GSSG). The cysteine–cystine reaction is known to proceed faster when Cys is already deprotonated (thiolated) (Soares Netto et al. 2007). Cys and GSH are the main antioxidants in living cells, controlling ROS. Thus, the mechanism described above for the vanadate/Cys oxi-reduction is not unexpected. Rather different is the mechanism which occurs between Cys and noble metal nanoparticles. Here the thiol side chain makes a covalent bond to the metal surface (Baptista et al. 2008), functionalizing the nanoparticle.

Additionally, we found out that the nanoparticles reduced by Cys slowly return to their original structure by the natural oxidation by oxygen from air. The yellowish color of the suspension reappears and the characteristic V_{10} signals in the ^{51}V NMR spectra return. This finding is very interesting, once it shows that the vanadium nanoparticles can be easily regenerated by a simple oxidation process and then turn on in another Cys determination. The cysteine formed in this reaction was found several days later at the bottom of the NMR tubule as a whitish deposit. Cysteine is known to be only slightly water soluble (Pontoni et al. 2000).

Cysteine is a very important aminoacid building block of proteins. Once the protein folds to its native

state, the bridging between cysteines is essential for protein geometry retention, since the S=S bond is responsible for joining adjacent protein segments. The geometry of a specific protein is fundamental for its biological function.

The detection of cysteine with V_2O_5 nanoparticles could find applications in the detection of folding/unfolding of proteins. Upon unfolding, the cysteines would be exposed and detected. This could be a far easier method than using more expensive detection techniques like Raman or Fourier Transform Infrared spectroscopies or NMR.

Since the detection of cysteine with V_2O_5 nanoparticles is selective, more complex biological samples like blood serum, albumin, urine, food additives or vegetals could be tested for cysteine.

Acknowledgments We acknowledge the support of CPqD—Centro de Pesquisa e Desenvolvimento em Telecomunicações and CNPq—Conselho de Desenvolvimento Científico e Tecnológico, Brazilian agencies.

References

Amendola V, Meneghetti M (2009) Laser ablation synthesis in solution and size manipulation of noble metal particles. Phys Chem Chem Phys 11:3805–3821

Baptista P, Pereira E, Eaton P, Doria G, Miranda A, Gomes I, Quaresma P, Franco R (2008) Gold nanoparticles for the development of clinical diagnosis methods. Anal Bioanal Chem 391:943–950

Celestino-Santos W, Bezerra AG Jr, Cezar AB, Mattoso N, Schreiner WH (2011) Vanadium oxide nanoparticles as optical sensors of cysteine. J Nanosci Nanotechnol 11: 4702–4707

Circu ML, Aw TY (2010) Reactive oxygen species, cellular redox systems and apoptosis. Free Radic Biol Med 48: 749–762

Crans DC, Baruah B, Ross A, Levinger NE (2009) Impact of confinement and interfaces on coordination chemistry: using oxovanadate reactions and proton transfer reactions as probes in reverse micelles. Coord Chem Rev 253:2178–2185

Forsters SM (2003) Diagnosing HIV infection. Clin Med 3: 203–205

Ji H, Zhu L, Liang D, Liu Y, Cai L, Zhang S, Liu S (2009) Use of a 12-molybdovanadate (V) modified ionic liquid carbon paste electrode as a bifunctional electrochemical sensor. Electrochim Acta 54:7429–7434

Krieger MA, Almeida E, Oelemann W, Lafaille JJ, Pereira JB, Krieger H, Carvalho MR, Goldenberg S (1992) Use of recombinant antigens for the accurate immunodiagnosis of Chagas' disease. Am J Trop Med Hyg 46:427–434

Lim II, Ip W, Crew E, Njoki PN, Mott D, Zhong CJ, Pan Y, Zhou S (2007) Homocysteine-mediated reactivity and assembly of gold nanoparticles. Langmuir 23:826–833

Lu C, Zu Y (2007) Specific detection of cysteine and homocysteine: recognizing one-methylene difference using fluorosurfactant-capped gold nanoparticles. Chem Commun 37:3871–3873

Ly TD, Laperche S, Brennan C, Vallari A, Ebel A, Hunt J, Martin L, Daghfal D, Schochetman G, Devare S (2004) Evaluation of the sensitivity and specificity of six HIV combined p24 antigen and antibody assays. J Virol Methods 122:185–194

Macara I, Kustin K, Cantley LC Jr (1980) Glutathione reduces cytoplasmic vanadate: mechanism and physiological implications. Biochim Biophys Acta 629:95–106

Maduraiveeran G, Ramaraj R (2011) Silver nanoparticles embedded in amine-functionalized silicate sol–gel network assembly for sensing cysteine, adenosine and NADH. J Nanopart Res 13:4267–4276

Pontoni G, Rotondo F, Spagnuolo G, Aurino MT, Cartèni-Farina M, Zappia V, Lama G (2000) Diagnosis and follow-up of cystinuria: use of proton magnetic resonance spectroscopy. Amino Acids 19:469–476

Quig D (1998) Cysteine metabolism and metal toxicity. Alt Med Rev 3:262–270

Ramasarma T (2003) The emerging redox profile of vanadium. Proc Indian Natl Acad Sci B69:649–672

Soares Netto LE, de Oliveira MA, Monteiro G, Demasi APD, Cussiol JRR, Discola KF, Demasi M, Silva GM, Alves SV, Faria VG, Horta BB (2007) Reactive cysteine in proteins: protein folding, antioxidant defense, redox signaling and more. Comp Biochem Physiol C 146:180–193

Summers MF, Henderson LE, Chance MR, Bess JW Jr, South TL, Blake PR, Sagi I, Perez-Alvarado G, Sowde RC III, Hare DR, Arthur LO (1992) Nucleocapsid zinc fingers detected in retroviruses: eXAFS studies of intact viruses and the solution-state structure of the nucleocapsid protein from HIV-1. Protein Sci 1:563–574

Tang S, Zhao J, Wang A, Viswanath R, Harma HR, Little RF, Yarchoan R, Stramer SL, Nyambi PN, Lee S, Wood O, Wong EY, Wang X, Hewlett IK (2010) Characterization of immune responses to capsid protein p24 of human immunodeficiency virus type 1 and implications for detection. Clin Vaccine Immunol 17:1244–1251

Teixeira MFS, Dockal ER, Cavalheiro ETG (2005) Sensor for cysteine based on oxovanadium (IV) complex of Salen modified carbon paste electrode. Sens Actuators B 106: 619–625

Thiagarajan S, Umasankar Y, Chen S-M (2010) Functionalized multi walled carbon nanotubes nano biocomposite film for the amperometric detection of L-cysteine. J Nanosci Nanotechnol 10:702–710

Wishart DS, Bigam CG, Holm A, Hodges RS, Sykes BD (1995) ^{1}H, ^{13}C and ^{15}N random coil NMR chemical shifts of the common amino acids. 1. Investigations of nearest-neighbor effects. J Biomol NMR 5:67–81

Wriedt HA (1989) The O–V (oxygen–vanadium) system. Bull Alloy Phase Diagrams 10:271–276

Zhang M, Yu M, Li F, Zhu M, Li M, Gao Y, Li L, Liu Z, Zhang J, Zhang D, Yi T, Huang C (2007) A highly selective fluorescence turn-on sensor for cysteine/homocysteine and its application in bioimaging. J Am Chem Soc 129:10322–10323